Accepted Manuscript

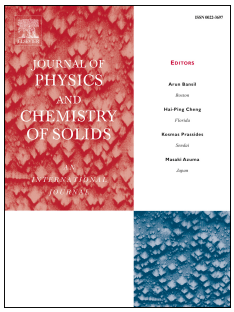

Incorporation of plasma-functionalized carbon nanostructures in composite laminates for interlaminar reinforcement and delamination crack monitoring

O.G. Kravchenko, D. Pedrazzoli, D. Kovtun, X. Qian, I. Manas-Zloczower

PII: S0022-3697(17)30486-9

DOI: 10.1016/j.jpcs.2017.09.018

Reference: PCS 8211

To appear in: *Journal of Physics and Chemistry of Solids*

Received Date: 3 April 2017

Revised Date: 4 September 2017

Accepted Date: 12 September 2017

Please cite this article as: O.G. Kravchenko, D. Pedrazzoli, D. Kovtun, X. Qian, I. Manas-Zloczower, Incorporation of plasma-functionalized carbon nanostructures in composite laminates for interlaminar reinforcement and delamination crack monitoring, *Journal of Physics and Chemistry of Solids* (2017), doi: 10.1016/j.jpcs.2017.09.018.

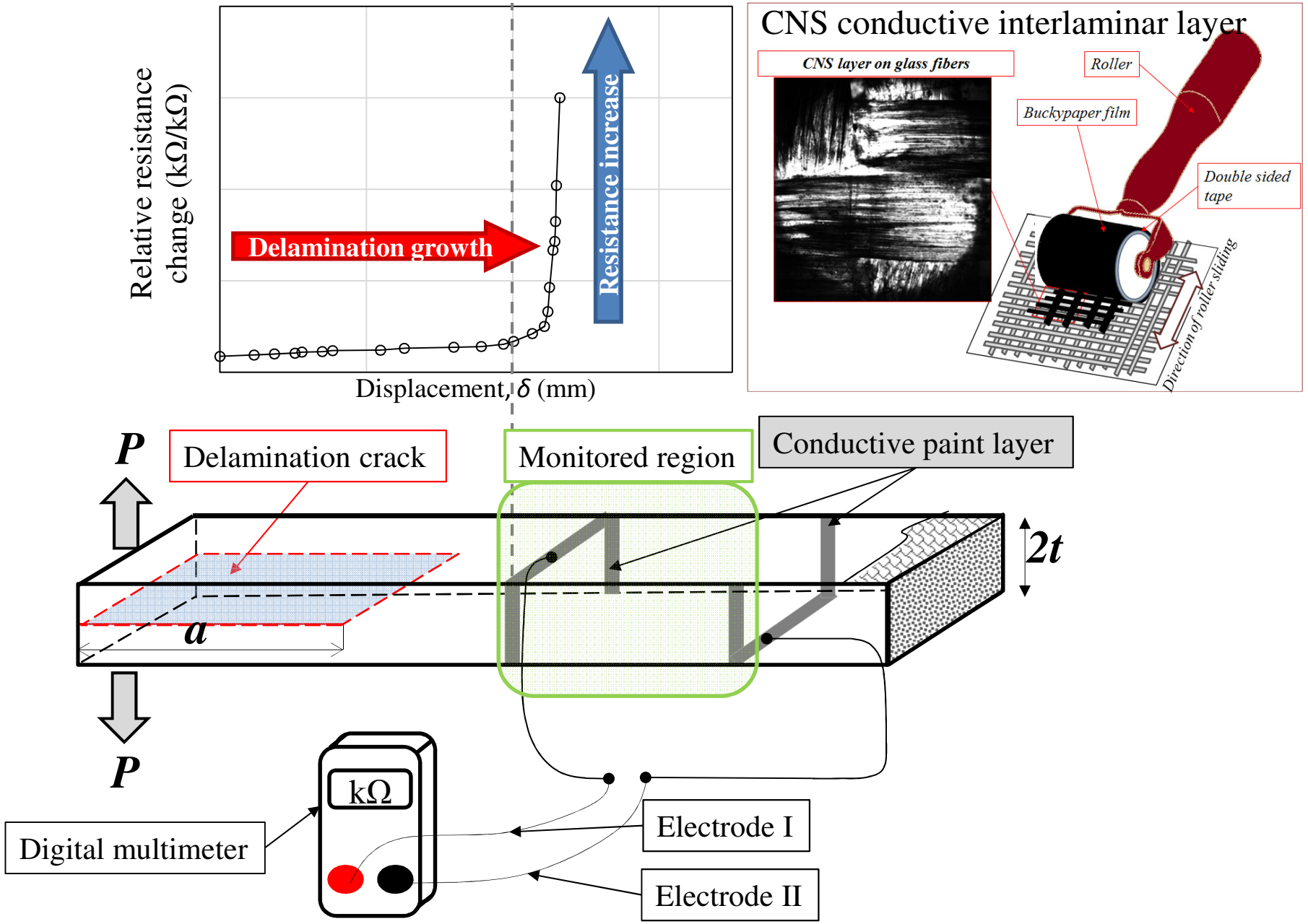
Relative resistance change (kΩ/kΩ)
Delamination growth
Resistance increase
Displacement, δ (mm)
CNS conductive interlaminar layer
CNS layer on glass fibers
Roller
Buckypaper film
Double sided tape
Direction of roller sliding
P
Delamination crack
Monitored region
Conductive paint layer
2t
a
P
kΩ
Digital multimeter
Electrode I
Electrode II

Incorporation of Plasma-Functionalized Carbon Nanostructures in Composite Laminates for Interlaminar Reinforcement and Delamination Crack Monitoring

O. G. Kravchenko[1*], D. Pedrazzoli[2], D. Kovtun[2], X. Qian[2], I. Manas-Zloczower[2]

[1] Department of Mechanical and Aerospace Engineering, Old Dominion University, Kaufman Hall, 4635 Hampton Blvd, VA 23529, United States

[2] Department of Macromolecular Science and Engineering, Case Western Reserve University, 2100 Adelbert Road, Cleveland, OH 44106-7202, United States

*Corresponding author.

E-mail address: okravche@odu.edu

Abstract

A new approach employing carbon nanostructure (CNS) buckypapers (BP) was used to prepare glass fiber/epoxy composite materials with enhanced resistance to delamination along with damage monitoring capability. The CNS-BP was subjected to plasma treatment to improve its wettability by epoxy and to promote stronger interfacial bonding. An increase up to 20% in interlaminar fracture toughness in mode I and mode II was observed in composite laminates incorporating CNS BP. Morphological analysis of the fracture surfaces indicated that failure in the conductive CNS layer provided a more effective energy dissipation mechanism, resulting in interlaminar fracture toughness increase. Moreover, fracture of the conductive CNS layer enabled damage monitoring of the composite by electrical resistance measurements upon delamination. The proposed approach provides multifunctional ply interphases, allowing to couple damage monitoring with interlaminar reinforcement of composite laminates.

Keywords:

Functional composites; Delamination; Fracture toughness, Plasma deposition; Damage monitoring; Carbon nanofillers

Introduction

Composite laminates combining glass fiber and thermosetting matrix is an important class of engineering structural materials which pose high mechanical in-plane properties and have found wide use in various engineering structures for aerospace, civil and wind power applications. One of the common design limitations for such materials is the occurrence of delamination cracks throughout the lifetime of the composite that leads to the loss of structural stiffness and eventually can threaten the structural integrity of the composite. The delamination can result from different precursors, including buckling, fatigue loading, low velocity impact, free-edge stresses, mounting and processing residual thermal stresses [1–3].

In order to avoid catastrophic failure of the composite laminate, delamination resistance can be improved adopting different strategies, by using stiff or rubbery inclusions as an interleave [4,5] or by through-thickness reinforcement in the form of rods or stitches [6–8]. Recently, the use of carbon nanotubes (CNT) has been explored as a way to reinforce thermosetting matrices in order to improve matrix-dominated failure modes including delamination behavior [9]. The resulting material presents a multi-scale structure as it incorporates fillers of different size and geometry. The use of CNTs in thermosetting matrices does not disrupt the fiber alignment and preserves high in-plane mechanical properties of the laminate. Selective reinforcement by CNTs in composite laminates using a

CNT layer at the interlaminar region of the laminate has been proposed to avoid problems associated with increased polymer viscosity and nanofiller dispersion in the matrix [10–15]. Delamination typically does not lead to immediate structural failure until a certain critical crack length is reached, therefore making structural health monitoring (SHM) of crack propagation an important problem of damage tolerance. Currently, there is a great demand for composite materials with enhanced resistance to delamination and damage monitoring capabilities [16,17]. Different approaches have been proposed for detecting delamination, including monitoring electrical impedance response of piezoelectric transducers [18,19], probing changes in natural frequencies of composite laminates [20], acoustic emission and thermography [21], use of embedded and surface-bonded fiber Bragg grating sensors [22,23]. Conductive carbon nanofillers at volume content above percolation were shown to be effective in monitoring damage initiation and propagation [24–27]. Methods of introducing nano-reinforcement can range from direct dispersion of CNTs in the polymeric matrix before fiber impregnation [26,28], use of CNT sheets between the plies [29,30], spraying CNT solution onto fiber mats [15,31] or by introducing CNT coating onto fiber surface [32,33].

The goal of this study is to present a new approach to create a layer of carbon nanofiller at ply interphases utilizing frictional roller sliding of buckypaper films. Buckypapers (BP) were prepared through vacuum-assisted filtration of highly cross-linked CNTs, further referred to as carbon nanostructures (CNS), which have recently been proposed as a practical and cost-effective solution in comparison to CNTs. In particular, CNS encapsulated flakes do not shed or produce respirable nanotubes when mixed with polymer matrices and can result in a uniform dispersion even at high filler loadings. The application

of CNS-BP circumvented using nanotube powder directly or dispersed in solvent and enabled a robust and scalable method for use in composite manufacturing processes. A layer of CNS was deposited at the interlaminar region of the impregnated woven glass fiber ply by frictional sliding of a BP film attached to the roller. The proposed approach allowed covering the area of glass fiber/epoxy ply over five times larger than the area of the BP itself. As such, the proposed approach allowed reduction in the amount of nanofiller used for reinforcement in the most critical region prone to delamination.

The proposed method enabled enhanced interlaminar mechanical properties and electrical conductivity of the composite, thus allowing damage monitoring capabilities of the composite. This approach coupled mechanical reinforcement and SHM allowing to detect delamination crack propagation.

Materials

Bi-directional E-glass woven fabrics (GF 4H satin weave) with areal density of 305 g/m^2 were supplied by FibreGlast. A bi-component epoxy resin (Sigma Aldrich) was used as matrix. In particular, an epoxy base (density = 1.16 g/cm^3, viscosity = 4000-6000 mPa·s), with Bisphenol A-diglycidyl-ether (equivalent epoxide weight (EEW) = 172-176 g·equiv.$^{-1}$), was mixed with a 5-Amino-1,3,3-trimethylcyclohexanemethylamine hardener (density = 0.92 g/cm^3) at a weight ratio of 100:24.5.

Carbon nanostructure (CNS) encapsulated flakes (Applied Nanostructured Solutions LLC) were used as filler to prepare BP. CNS were produced as cross-linked multiwall carbon nanotubes and encapsulated in flakes using polyethylene glycol as a surfactant. BP were prepared following a methodology previously optimized in our group [34]. Specifically,

CNS-BP were prepared by sonicating a given amount of CNS in isopropyl alcohol for 10 min (Fig. 1a), using a Sonics Materials Vibra Cell VCX500 (60% amplitude, 13 mm probe). The suspension was then filtrated through a Millipore vacuum filtration assembly with nitrocellulose filter (pore size= 0.8 μm). After vacuum filtration, the CNS-BP films wet cakes were dried in a vacuum oven for 6h at 100°C. CNS-BP with diameter of 70 mm and average thickness 50-75μm were used to create a CNS layer on the woven glass fiber ply impregnated with epoxy matrix. CNS-BP was attached to the roller by using double sided adhesive tape (Fig. 1a). Next, the roller with BP was applied to the impregnated surface of the GF. Due to frictional forces induced by the rolling motion the CNS agglomerates detached from the buckypaper and adhered to the composite forming homogeneous CNS layer. The CNS agglomerates covered an area of the composite lamina 5 times larger than the area of the buckypaper itself with an average coating thickness below 10 μm. Consequently, the proposed method allowed a cost effective way of introducing carbon nanofillers onto the surface of the composite, by comparison with using the buckypaper directly.

The epoxy base was manually mixed with the hardener for 2 minutes and degassed under vacuum for 20 min. This mixture was then used to prepare composites by wet hand lay-up of 14 plies. A layer coating of CNS filler was deposited via frictional roller sliding (Fig. 1b) at the laminate midplane, namely top and bottom surfaces of 7^{th} and 8^{th} ply, respectively, for interlaminar fracture toughness testing. Noteworthy, the created CNS layer on the GF appeared to be formed by overlapping CNS agglomerates, as shown in Fig. 1b. A thin CNS layer covering the prepreg surface allowed to avoid any impregnation problems, otherwise

difficult due to the low permeability of the BP film [35]. A thin film (~12.5 μm) of polytetrafluoroethylene (PTFE) was also placed at the midplane to serve as an insert for an initial crack. Composite laminates were thermally cured, according to the typically recommended two stage cure cycle conditions for epoxy based composites, namely 2 h at 90 °C followed by 2 h at 180 °C, while applying 80 psi pressure with the Carver laboratory press during the second stage [36].

2. Methods

2.2.1 Surface modification of buckypaper by plasma treatment

Oxygen plasma treatment was performed with the aim of inducing oxygen-functional groups on the BP surfaces to promote stronger chemical bonding between the BP and the epoxy matrix [37–39]. Functionalization was done using a plasma reactive ion etcher (Plasma Etch PE-100-RIE) flowing O_2 (OX-UHP300) at 20 sccm (standard cubic centimeter per minute). BPs were exposed to the plasma at room temperature under a pressure of 13.3 Pa (0.1 Torr), applying a load of 30W for 2 min in order to achieve homogeneous surface treatment and limit surface etching. Since previous investigations indicated that even for prolonged times of treatment the penetration depth is around 20-30 μm (corresponding to about the BP midplane), both sides of the BP were treated for 2 min.

2.2.2 X-ray photoelectron spectroscopy

Surface analysis of the BP was performed by X-ray photoelectron spectroscopy (XPS) using a PHI VeraProbe 5000 XPS, adopting a monochromatic AlKα radiation ($h\nu$ = 1486.6

eV, power = 100W, neutralizer of 1.3 eV at 20 μA) using a beam diameter of 100 μm with emission angle of 90° and under a pressure of 10^{-10} mbar. The BP was analyzed on the outer surface as well as on the inner surface in order to quantify the functionalization gradient through its thickness. Inner surfaces were obtained by cleaving the BP using scotch tape on both sides of the BP. Noteworthy, the inner surface obtained after cleavage was about at the midplane of the BP, as measured using a micrometer caliper. The obtained XPS spectra were analyzed in FAT mode and deconvoluted by VersaProbe software.

2.2.3 Surface wettability analysis

Wettability measurements were performed using a static contact angle measurement setup. At least five measurements were carried out by depositing a microdroplet (3 μl) of DI water on the surface of the BP before and after plasma treatment. Contact angle values were determined with a manual contact angle goniometer (Ramé-Hart Inc.).

2.2.4 Mode I and mode II interlaminar fracture toughness testing

Composite laminates consisting of 14 plies were prepared for interlaminar fracture toughness testing in mode I and II. The composite plate incorporated a PTFE insert to serve as crack initiator. Half of the plate at the midplane was coated with CNS-BP layer as described in the previous section. This procedure allowed manufacturing double cantilever beam (DCB) specimens for mode I testing with and without CNS layer, denoted as Mode *I*-neat and Mode *I*-CNS respectively from a single laminate plate. A similar procedure was used to prepare an end notch flexure specimen (ENF) for mode II testing using three point

bending loading conditions. The dimensions and test conditions were adopted from ASTM-D5528-01 [40]. Specimens presented an initial crack length, *a*, of approximately 40 mm. The CNS layer in the CNS-samples was located after the initial crack tip. Piano hinges were bonded to the outer faces of the specimens at the cracked ends using an epoxy paste adhesive (LORD 310 A/B). Specimen edges were coated with a white spray primer to improve the visibility of the crack tip during testing. Moreover, a printed scale was applied to the edge of the specimen in order to provide a reference for the measurement of the crack length.

Specimens were tested in mode I and II fracture toughness on a MTS electro-mechanic universal testing machine at a rate of 3 mm/min while acquiring the load-displacement data at 10 Hz. The crack advancement was monitored by taking consecutive pictures using a Mighty Scope 5.0M Digital Microscope (Aven). In particular, each specimen was loaded until the applied load reached a critical value corresponding to visual detection of crack propagation using the digital microscope. The crack length was measured from the load application point to the location of the crack tip prior to crack propagation. Multiple loading cycles were conducted, following ASTM recommended procedure for unloading the sample [40], to determine the effect of the CNS layer on the interlaminar fracture toughness of the composite and to enable monitoring composite electrical resistance (ER) during crack propagation. The crack propagation between different loading cycles in Mode I testing typically ranged between 3-5 mm. Calculation of the critical energy release rate, ERR, for mode I and II fracture toughness (G_{IC} and G_{IIC}, respectively) was done using the following beam model expressions [40]:

$$G_{Ic} = \frac{3\,P_c\,\delta_c}{2\,w\,\cdot a} \quad (1)$$

$$G_{IIC} = \frac{9P_c{}^2a^2C}{4wL^3(1+1.5(a/L)^3)} \quad (2)$$

where P_c is the critical maximum force; δ_c is the corresponding critical displacement; ?? is DCB width; ?? is DCB crack length; C is beam compliance determined from the experimental load-displacement curve; L is a half-span of ENF sample.

These calculations for neat composite samples and samples with CNS layer at the midplane provided quantitative evaluation of the delamination resistance.

2.2.5 Monitoring of composite resistance during delamination growth

The incorporation of the conductive CNS layer at the interlaminar region enabled monitoring changes in the electrical resistance (ER) of the composite laminate during crack propagation. The ER was monitored along the sample using a Fluke 72 series II digital multimeter configured according to the setup presented in Fig. 2. In particular, a suspension of silver nanoparticles (Pelco® colloidal silver liquid) was used to paint layers of silver paint (width *(d)* ~ 2mm) on opposing edges of the specimen and connect them to layers on the top and bottom surfaces of the specimen. The first layer of paint was located ahead of the initial PTFE insert at a distance of 15 mm, and the distance between the first and second layer was about 20 mm. Copper wires were fixed to the silver paint layer of each electrode as shown in Fig. 2 using a conductive epoxy paste (Duralco™ 125 epoxy kit). Electrical resistance was continuously recorded during each loading test to allow correlating delamination crack propagation with changes in ER.

3. Results and Discussion

3.1 Effect of plasma functionalization on the buckypaper surface properties

XPS analyses indicated significant changes in the surface chemistry on the outer and inner surfaces of the BP after plasma functionalization. The C1s spectra were deconvoluted into five characteristic Gaussian peaks (Fig. 3) characterized by sp^2-hybridized graphite-like carbon atoms (284.6 ± 0.1 eV), sp^3-hybridized graphite-like carbon atoms (285.7 ± 0.1 eV), C-O (286.6 ± 0.2 eV), C=O (287.4 ± 0.2 eV) and O-C=O (288.4 ± 0.2 eV). Analysis of the C1s spectra indicated noticeable changes in the intensity of peaks relative to different chemical bonds, in particular, C-O, C=O and O-C=O bonds upon plasma treatment. It has been reported that plasma treatment gives rise to hydroxyl and carboxyl functional groups at the CNT surface as a result of O_2 dissociation on vacancies created during the plasma treatment [37,41,42]. Concurrently, the graphitic structure (C=C) was disrupted at the expense of the C-C groups due to plasma excitation. This change was also reflected in the decrease in $\pi \rightarrow \pi^*$ transition (indicating the promotion of an electron from a π-bonding orbital to an antibonding π orbital* occurring due to a raise in the ground state energy). The C/O atomic ratio significantly changed, indicating that plasma treatment was effective in inducing oxygen functional groups on the BP surfaces. This change in C/O atomic ratio is typically associated with increased hydrophilicity and wettability of the treated surfaces [37]. Contact angle measurements performed on the BP surface before and after plasma treatment showed that untreated BP surfaces exhibited hydrophobic characteristics (contact angle = 129 ± 1°), while the treated BP films were highly hydrophilic (water microdroplets were completely adsorbed on the BP surface). Concurrently, such oxygen functional groups

covalently attached to the CNS offer the opportunity for chemical interactions with the epoxy system. It is known from the literature that epoxy groups can directly react with hydroxyl and carboxylic groups forming strong covalent bonds [43,44]. In particular, epoxy reacting with carboxyl can form esters, while in the presence of tertiary amines, epoxy groups are also capable of reacting with hydroxyl groups to form ether linkages. Therefore, hydroxyl and carboxylic functional groups implanted onto the CNS by plasma treatment can provide an in situ chemical integration of the nanotubes into the amine/epoxy system. This type of interactions could strengthen the interfacial bonding between CNS and the matrix, as similar chemical reactions have been previously observed in traditional carbon fiber/epoxy interfaces [45]. Stronger interfacial bonding between epoxy and CNS could promote more efficient stress transfer from the matrix to the glass fibers and improve the mechanical properties of the composite [46]. It is important to point out that initial attempts were made to integrate BP directly in the composite laminate, however, poor impregnation of BP during manufacturing led to reduced interlaminar properties, showing adhesive failure of the BP. However, plasma treated BP showed better adherence to the composite and the mechanism of failure was cohesive. Consequently , the results presented in the following sections were obtained using plasma treated CNS-BP incorporated into the composite using frictional roller sliding, which improved impregnation enabling cohesive fracture in the CNS layer. As discussed further, cohesive fracture of CNS was found beneficial for delamination crack monitoring. The surface resistivity of the CNS-BP, measured according to the ASTM D-257 standard using a Prostat® PRF-912B miniature concentric ring fixture set, was $(7.6 \pm 0.4) \cdot 10^0$ Ω/sq and $(10.8 \pm 1.8) \cdot 10^0$ Ω/sq for untreated

and plasma-treated CNS-BP, respectively. Measurements were carried out at room temperature at around 50% relative humidity and repeated on at least 5 different areas of the film. The electrical resistivity of CNS-BP was thus sufficiently low to enable monitoring of the composite resistance upon delamination.

3.2 Experimental results for mode I and mode II testing

The results of mode I and II interlaminar fracture toughness indicated an increase up to 20% in delamination resistance in composite laminates with plasma treated CNS-BP layer at the interlaminar region, as shown in Fig. 4. The experimental results were found to be statistically significant at $p<0.05$ by conducting the t-test using two-tailed hypothesis, which yielded a *p*-value of 6.6E-3.

The more pronounced resistance curve (R-curve) behavior in mode I was found in samples with CNS-BP layer at the interlaminar midplane region (Figure 5). The increased delamination resistance can be explained in terms of the mixed cohesive/adhesive mode of fracture of the CNS layer observed after examining the fracture surface (Figure 6a). The area covered with CNS on the post-mortem top and bottom fracture surfaces of the DCB sample, estimated using image processing analysis (ImageJ), was similar indicating a combination of cohesive/adhesive fracture (Figure 6b). The crack pinning occurring when the crack front encounters rigid inclusions during propagation was shown to contribute to the improved toughness of polymeric systems with stiff inclusions [47,48]. This fracture mechanism explains the improved G_{IC} results in the present case. The irregular shapes of CNS coverage on the fracture surfaces indicate complex crack propagation path during delamination growth. Scanning electron micrographs of the fracture surface (Figure 7) also

show microscopic CNS agglomerates breaking the conductive paths upon delamination, and, as discussed in the next section, inducing changes in the composite ER.

3.3 Delamination crack monitoring using composite electrical resistance

The electrical resistance was monitored during opening displacement (δ) of the DCB sample under mode I loading conditions as shown in Figure 8. After crack propagation was visually detected using microscopy, the test was stopped and the sample was unloaded following the ASTM recommended procedure. Since the crack propagation in the DCB sample is stable in a displacement controlled test, crack advancement occurs incrementally with the reduction in the critical load necessary to further propagate the crack. Therefore, the unloading procedure allowed to monitor the ER response of the composite upon different opening displacements of the DCB sample for a given crack length. Each "loading/unloading" cycle was labeled as "Test". No noticeable change in ER was observed before the crack reached the location of paint layer "*I*", indicative of the beginning of the ER monitoring region. When the crack reached the paint layer "*I*" (between Test-7 and Test-8) the ER spiked. During the unloading cycles, after Test-7 some electrical conductivity was recovered due to crack closure, however without reaching the pristine undamaged electrical conductivity. Shortly after the crack propagated and passed the location of paint layer "*I*", the ER continued to increase rapidly at the end of Test-8. Once the delamination propagated into the monitoring region (between conductive paint layer "*I*" and "*II*") a significant increase in composite resistance (by 200-300%) developed. The significant change in ER was attributed to delamination propagation through the conductive CNS layer and breaking of the conductive path as was seen from the fractured surfaces in

Fig. 6. The cohesive/adhesive fracture behavior of the interleave was responsible for promoting crack pinning and deflection which resulted in increased critical energy release rate, while the electrically conductive CNS layer also enabled damage monitoring.

Conclusions

A layer of conductive filler was introduced in the glass fiber/epoxy composite laminate by frictional roller sliding of a CNS-BP film on the laminate surface creating a layer of CNS. Surface functionalization of the CNS-BP was achieved by oxygen plasma treatment which improved hydrophilicity as observed using contact angle measurements. Plasma treatment provided active polar groups on the surface and interior of CNS-BP films, strengthening interfacial bonding with the epoxy matrix and improving impregnation of CNS.

The CNS-BP layer incorporated in the composite was found to promote functionality in the multi-scale composite by coupling enhanced mechanical properties with sufficiently high electrical conductivity. Improved resistance to delamination both in mode I and II was observed in multi-scale composites with CNS-BP layer. The improved interlaminar toughness was attributed to the cohesive/adhesive fracture of the CNS layer, while the discontinuous CNS pattern on the fracture surface also enabled monitoring the delamination propagation.

This study presents a new approach of creating a layer of carbon nanofiller at ply interphases by frictional roller sliding of buckypaper films onto the impregnated woven glass fiber plies. The novelty of the approach consists in circumventing the dispersion of nanotube powder in the epoxy and enabling a robust and scalable method for use in composite manufacturing processes. The interlaminar mechanical properties of the

composite were enhanced, while allowing also damage monitoring through changes in electrical resistance of the carbon nanofiller layer. The proposed method of enabling mechanical and electrical functionality of ply interphases in composite laminates provides an efficient and cost-effective tool in designing laminates with improved interlaminar mechanical properties and delamination sensing capabilities.

Acknowledgement

We acknowledge the National Science Foundation for financial support of our research through PIRE-1243313 grant. The authors acknowledge Applied Nanostructured Solutions LLC for providing the CNS materials used in this work. The authors also would like to thank Dr. Ina Martin (Case Western Reserve University, Department of Materials Science and Engineering, MORE center) for her support during plasma treatments. Special thanks to Dr. Wayne Jennings (Case Western Reserve University, Department of Materials Science and Engineering, SCSAM center) for his help with XPS analyses. Acknowledgements are also due to Dr. Imre Treufeld (Case Western Reserve University, Department of Chemistry) for his valuable help with some aspects of the experimental work and Dr. Marriner Merrill (U.S. Naval Research Laboratory) for his help with SEM.

References

1. Sela, N., and Ishai, O., "Interlaminar fracture toughness and toughening of laminated composite materials: a review," *Composites*, vol. 20, Sep. 1989, pp. 423–435.
2. Goodsell, J., Pagano, N. J., Kravchenko, O., and Byron Pipes, R., "Interlaminar Stresses in Composite Laminates Subjected to Anticlastic Bending Deformation," *Journal of Applied Mechanics*, vol. 80, May 2013, pp. 041020–041020.
3. Kravchenko, O. G., Kravchenko, S. G., and Pipes, R. B., "Chemical and thermal shrinkage in thermosetting prepreg," *Composites Part A: Applied Science and Manufacturing*, vol. 80, 2016, pp. 72–81.
4. Yasaee, M., Bond, I. P., Trask, R. S., and Greenhalgh, E. S., "Mode I interfacial toughening through discontinuous interleaves for damage suppression and control," *Composites Part A: Applied Science and Manufacturing*, vol. 43, Jan. 2012, pp. 198–207.
5. Singh, S., and Partridge, I. K., "Mixed-mode fracture in an interleaved carbon-fibre/epoxy composite," *Composites Science and Technology*, vol. 55, 1995, pp. 319–327.
6. Zhang, B., Allegri, G., and Hallett, S. R., "An experimental investigation into multi-functional Z-pinned composite laminates," *Materials & Design*, vol. 108, Oct. 2016, pp. 679–688.
7. Mouritz, A. P., Bannister, M. K., Falzon, P. J., and Leong, K. H., "Review of applications for advanced three-dimensional fibre textile composites," *Composites Part A: Applied Science and Manufacturing*, vol. 30, Dec. 1999, pp. 1445–1461.
8. Kravchenko, S., Kravchenko, O., Wortmann, M., Pietrek, M., Horst, P., and Pipes, R. B., "Composite toughness enhancement with interlaminar reinforcement," *Composites Part A: Applied Science and Manufacturing*, vol. 54, 2013, pp. 98–106.
9. Qian, H., Greenhalgh, E. S., Shaffer, M. S. P., and Bismarck, A., "Carbon nanotube-based hierarchical composites: a review," *Journal of Materials Chemistry*, vol. 20, Jun. 2010, pp. 4751–4762.
10. Arai, M., Noro, Y., Sugimoto, K., and Endo, M., "Mode I and mode II interlaminar fracture toughness of CFRP laminates toughened by carbon nanofiber interlayer," *Composites Science and Technology*, vol. 68, Feb. 2008, pp. 516–525.
11. Garcia, E. J., Wardle, B. L., and John Hart, A., "Joining prepreg composite interfaces with aligned carbon nanotubes," *Composites Part A: Applied Science and Manufacturing*, vol. 39, Jun. 2008, pp. 1065–1070.
12. Sager, R. J., Klein, P. J., Davis, D. C., Lagoudas, D. C., Warren, G. L., and Sue, H.-J., "Interlaminar fracture toughness of woven fabric composite laminates with carbon nanotube/epoxy interleaf films," *Journal of Applied Polymer Science*, vol. 121, Aug. 2011, pp. 2394–2405.
13. Khan, S. U., and Kim, J.-K., "Improved interlaminar shear properties of multiscale carbon fiber composites with bucky paper interleaves made from carbon nanofibers," *Carbon*, vol. 50, Nov. 2012, pp. 5265–5277.
14. Williams, J., Graddage, N., and Rahatekar, S., "Effects of plasma modified carbon nanotube interlaminar coating on crack propagation in glass epoxy composites,"

Composites Part A: Applied Science and Manufacturing, vol. 54, Nov. 2013, pp. 173–181.

15. Zhang, H., Liu, Y., Kuwata, M., Bilotti, E., and Peijs, T., "Improved fracture toughness and integrated damage sensing capability by spray coated CNTs on carbon fibre prepreg," *Composites Part A: Applied Science and Manufacturing*, vol. 70, Mar. 2015, pp. 102–110.
16. Roach, D., Rackow, K., DeLong, W., Yepez, S., Reedy, D., and White, S., "Use of Composite Materials, Health Monitoring and Self-Healing Concepts to Refurbish Our Civil and Military Infrastructure."
17. Dyas, S. J., Scheidler, J., Taylor, S. G., Farinholt, K., and Park, G., "Structural Health Monitoring of Wind Turbine Blades Under Fatigue Loads," *Topics in Experimental Dynamics Substructuring and Wind Turbine Dynamics, Volume 2*, R. Mayes, D. Rixen, D.T. Griffith, D.D. Klerk, S. Chauhan, S.N. Voormeeren, and M.S. Allen, eds., Springer New York, 2012, pp. 227–245.
18. Bois, C., Herzog, P., and Hochard, C., "Monitoring a delamination in a laminated composite beam using in-situ measurements and parametric identification," *Journal of Sound and Vibration*, vol. 299, Feb. 2007, pp. 786–805.
19. Alaimo, A., Milazzo, A., and Orlando, C., "A Strain Sensing Structural Health Monitoring System for Delaminated Composite Structures," *Applied Mechanics and Materials*, vol. 249–250, Dec. 2012, pp. 849–855.
20. Doebling, S. W., Farrar, C. R., Prime, M. B., and Shevitz, D. W., *Damage Identification and Health Monitoring of Structural and Mechanical Systems from Changes in Their Vibration Characteristics: A Literature Review*, Los Alamos National Lab., NM (United States), 1996.
21. Amenabar, I., Mendikute, A., López-Arraiza, A., Lizaranzu, M., and Aurrekoetxea, J., "Comparison and analysis of non-destructive testing techniques suitable for delamination inspection in wind turbine blades," *Composites Part B: Engineering*, vol. 42, Jul. 2011, pp. 1298–1305.
22. Palaniappan, J., Wang, H., Ogin, S. L., Thorne, A., Reed, G. T., Tjin, S. C., and McCartney, L. N., "Prediction of the reflected spectra from chirped fibre Bragg gratings embedded within cracked crossply laminates," *Measurement Science and Technology*, vol. 17, 2006, p. 1609.
23. Ogin, S. L., Sanderson, A. R., Crocombe, A. D., Gower, M. R. L., Lee, R. J., Tjin, S. C., and Lin, B., "Monitoring crack growth in a DCB test using a surface-bonded chirped FBG sensor," Jeju, Korea,: 2011.
24. Zhang, H., Bilotti, E., and Peijs, T., "The use of carbon nanotubes for damage sensing and structural health monitoring in laminated composites: a review," *Nanocomposites*, vol. 1, Oct. 2015, pp. 167–184.
25. Thostenson, E. T., and Chou, T.-W., "Carbon Nanotube Networks: Sensing of Distributed Strain and Damage for Life Prediction and Self Healing," *Advanced Materials*, vol. 18, Nov. 2006, pp. 2837–2841.
26. Böger, L., Wichmann, M. H. G., Meyer, L. O., and Schulte, K., "Load and health monitoring in glass fibre reinforced composites with an electrically conductive nanocomposite epoxy matrix," *Composites Science and Technology*, vol. 68, Jun. 2008, pp. 1886–1894.

27. Abot, J. L., Song, Y., Vatsavaya, M. S., Medikonda, S., Kier, Z., Jayasinghe, C., Rooy, N., Shanov, V. N., and Schulz, M. J., "Delamination detection with carbon nanotube thread in self-sensing composite materials," *Composites Science and Technology*, vol. 70, Jul. 2010, pp. 1113–1119.
28. Pedrazzoli, D., Dorigato, A., and Pegoretti, A., "Monitoring the mechanical behavior under ramp and creep conditions of electrically conductive polymer composites," *Composites Part A: Applied Science and Manufacturing*, vol. 43, Aug. 2012, pp. 1285–1292.
29. Liu, L., Wu, J., and Zhou, Y., "Enhanced delamination initiation stress and monitoring sensitivity of quasi-isotropic laminates under in-plane tension by interleaving with CNT buckypaper," *Composites Part A: Applied Science and Manufacturing*, vol. 89, Oct. 2016, pp. 10–17.
30. Aly, K., Li, A., and Bradford, P. D., "Strain sensing in composites using aligned carbon nanotube sheets embedded in the interlaminar region," *Composites Part A: Applied Science and Manufacturing*, vol. 90, Nov. 2016, pp. 536–548.
31. Nag-Chowdhury, S., Bellegou, H., Pillin, I., Castro, M., Longrais, P., and Feller, J. F., "Non-intrusive health monitoring of infused composites with embedded carbon quantum piezo-resistive sensors," *Composites Science and Technology*, vol. 123, Feb. 2016, pp. 286–294.
32. Sebastian, J., Schehl, N., Bouchard, M., Boehle, M., Li, L., Lagounov, A., and Lafdi, K., "Health monitoring of structural composites with embedded carbon nanotube coated glass fiber sensors," *Carbon*, vol. 66, Jan. 2014, pp. 191–200.
33. Wiegand, N., and Mäder, E., "Multifunctional Interphases: Percolation Behavior, Interphase Modification, and Electro-Mechanical Response of Carbon Nanotubes in Glass Fiber Polypropylene Composites," *Advanced Engineering Materials*, vol. 18, Mar. 2016, pp. 376–384.
34. Meng, Q., and Manas-Zloczower, I., "Carbon nanotubes enhanced cellulose nanocrystals films with tailorable electrical conductivity," *Composites Science and Technology*, vol. 120, Dec. 2015, pp. 1–8.
35. Click, B. M., "Carbon Nanotube Buckypaper Permeability and Prepreg Process Study," 2016.
36. Kravchenko, O. G., Kravchenko, S. G., and Pipes, R. B., "Cure history dependence of residual deformation in a thermosetting laminate," *Composites Part A: Applied Science and Manufacturing*, vol. 99, pp. 186–197.
37. Jiang, Q., Li, Y., Xie, J., Sun, J., Hui, D., and Qiu, Y., "Plasma functionalization of bucky paper and its composite with phenylethynyl-terminated polyimide," *Composites Part B: Engineering*, vol. 45, Feb. 2013, pp. 1275–1281.
38. Li, R., Ye, L., and Mai, Y.-W., "Application of plasma technologies in fibre-reinforced polymer composites: a review of recent developments," *Composites Part A: Applied Science and Manufacturing*, vol. 28, Jan. 1997, pp. 73–86.
39. Liston, E. M., "Plasma Treatment for Improved Bonding: A Review," *The Journal of Adhesion*, vol. 30, Jan. 1989, pp. 199–218.
40. "ASTM D5528-13, Standard Test Method for Mode I Interlaminar Fracture Toughness of Unidirectional Fiber-Reinforced Polymer Matrix Composites, ASTM International, West Conshohocken, PA, 2013, www.astm.org."

41. Felten, A., Bittencourt, C., and Pireaux, J. J., "Gold clusters on oxygen plasma functionalized carbon nanotubes: XPS and TEM studies," *Nanotechnology*, vol. 17, 2006, p. 1954.
42. Zschoerper, N. P., Katzenmaier, V., Vohrer, U., Haupt, M., Oehr, C., and Hirth, T., "Analytical investigation of the composition of plasma-induced functional groups on carbon nanotube sheets," *Carbon*, vol. 47, Aug. 2009, pp. 2174–2185.
43. Zhu, J., Kim, J., Peng, H., Margrave, J. L., Khabashesku, V. N., and Barrera, E. V., "Improving the Dispersion and Integration of Single-Walled Carbon Nanotubes in Epoxy Composites through Functionalization," *Nano Letters*, vol. 3, Aug. 2003, pp. 1107–1113.
44. Ritts, A. C., Yu, Q., Li, H., Lombardo, S. J., Han, X., Xia, Z., and Lian, J., "Plasma Treated Multi-Walled Carbon Nanotubes (MWCNTs) for Epoxy Nanocomposites," *Polymers*, vol. 3, Dec. 2011, pp. 2142–2155.
45. Jones, C., "Special Issue Interfaces in Composites The chemistry of carbon fibre surfaces and its effect on interfacial phenomena in fibre/epoxy composites," *Composites Science and Technology*, vol. 42, Jan. 1991, pp. 275–298.
46. Garg, M., Sharma, S., and Mehta, R., "Pristine and amino functionalized carbon nanotubes reinforced glass fiber epoxy composites," *Composites Part A: Applied Science and Manufacturing*, vol. 76, Sep. 2015, pp. 92–101.
47. Kinloch, A. J., *Fracture Behaviour of Polymers*, Springer Science & Business Media, 2013.
48. Lange, F. F., and Radford, K. C., "Fracture energy of an epoxy composite system," *Journal of Materials Science*, vol. 6, Sep. 1971, pp. 1197–1203.

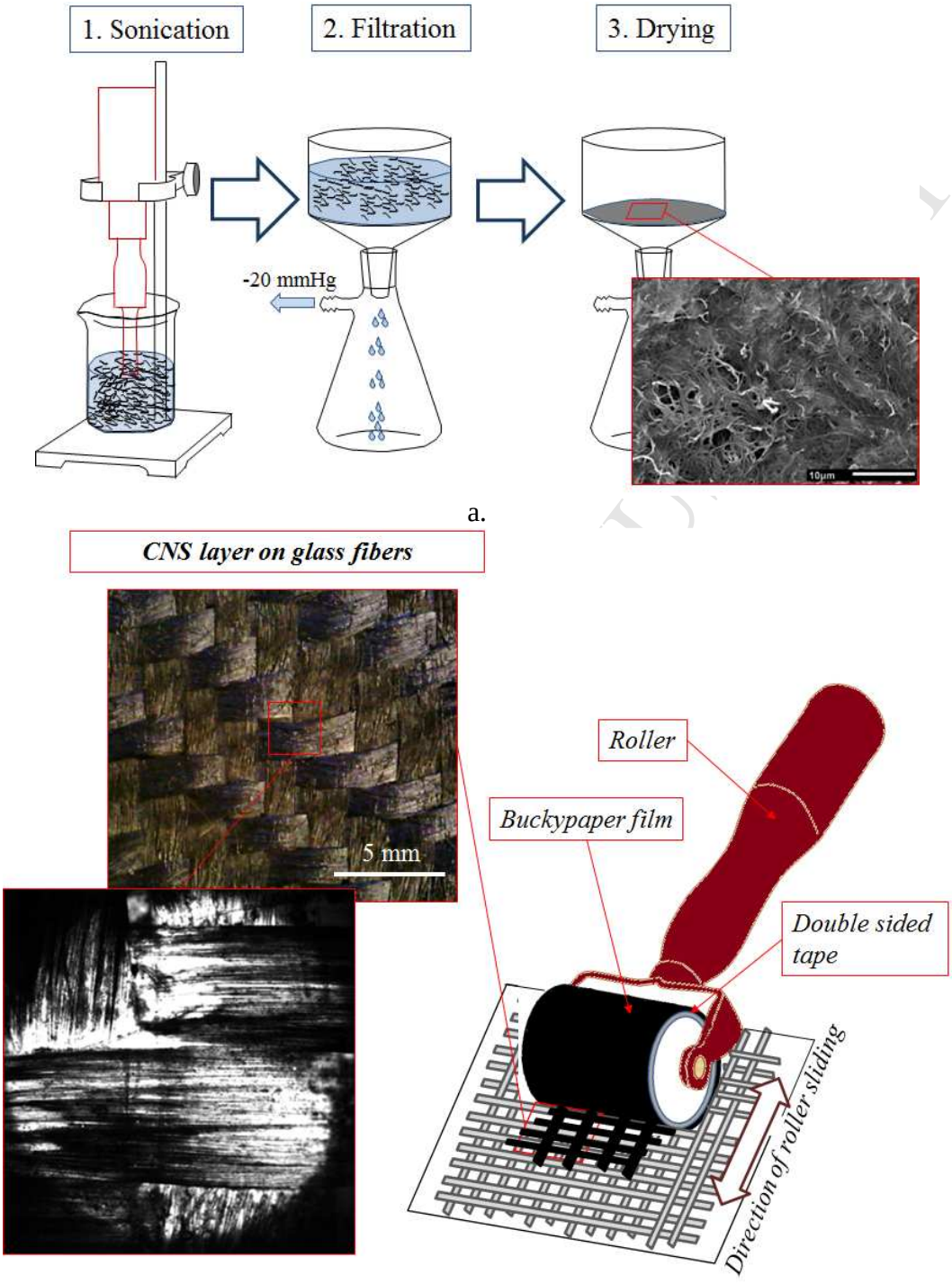

Figure 1. Schematics of buckypaper preparation (a) and frictional sliding deposition of CNS layer on the glass fibers (b)

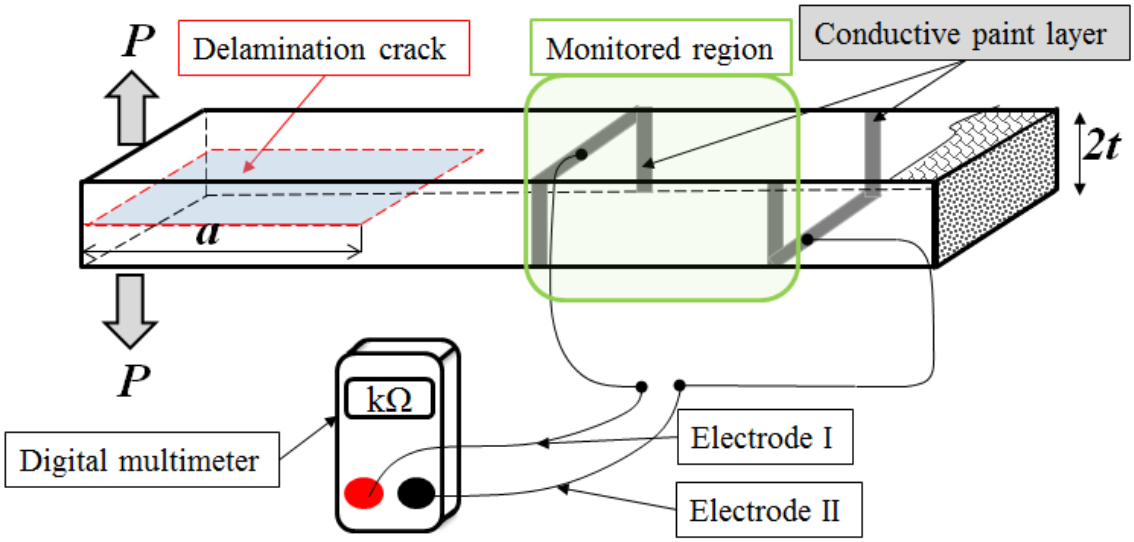

Figure 2. Schematics of double cantilever beam loading conditions and electrodes for resistance measurement

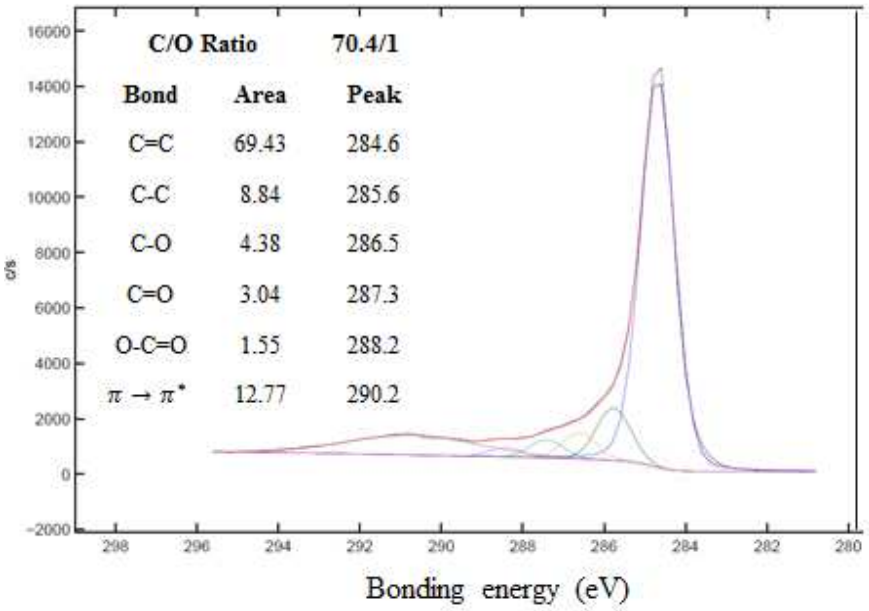
C/O Ratio 70.4/1
Bond Area Peak
C=C 69.43 284.6
C-C 8.84 285.6
C-O 4.38 286.5
C=O 3.04 287.3
O-C=O 1.55 288.2
π → π* 12.77 290.2
c/s
Bonding energy (eV)

a.

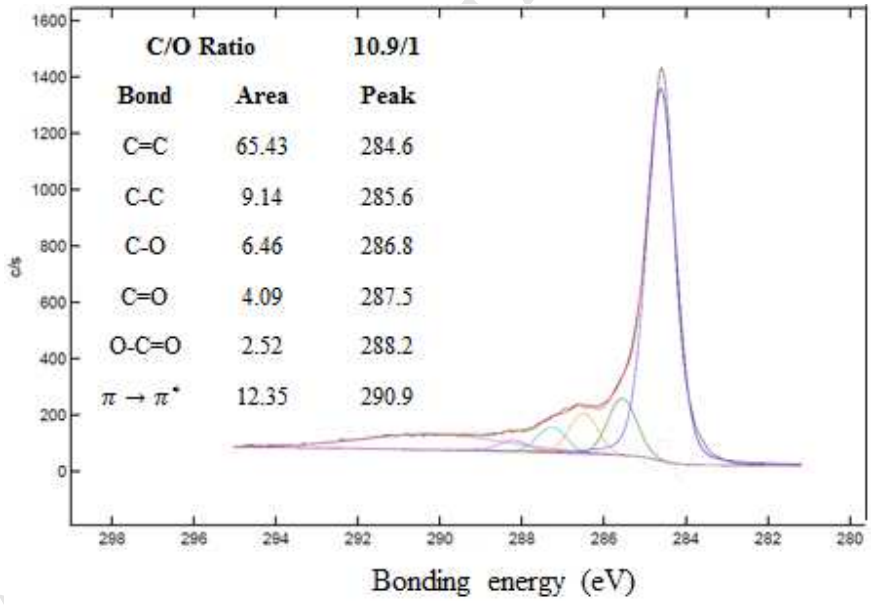
C/O Ratio 10.9/1
Bond Area Peak
C=C 65.43 284.6
C-C 9.14 285.6
C-O 6.46 286.8
C=O 4.09 287.5
O-C=O 2.52 288.2
π → π* 12.35 290.9
c/s
Bonding energy (eV)

b.

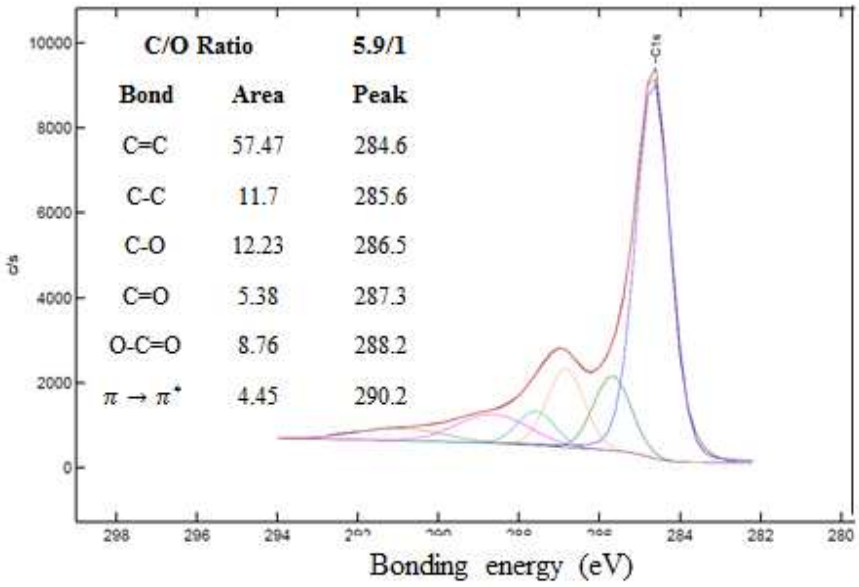

c.

Figure 3. C1s spectra obtained by XPS analysis indicating the atomic carbon-to-oxygen ratio of the untreated BP (a), inner cleaved surface (b) and exterior surface (c) of plasma-treated BP

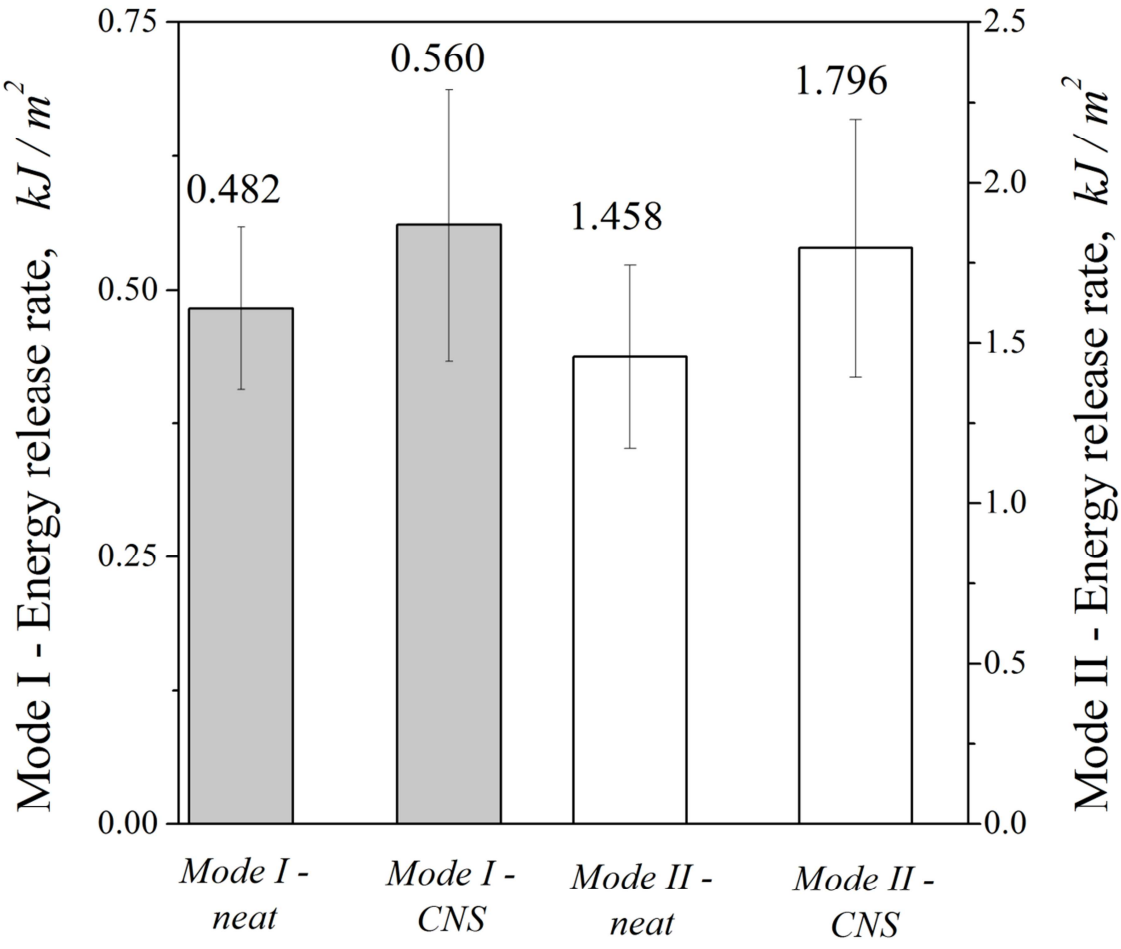

Figure 4. Mode I and II interlaminar toughness results

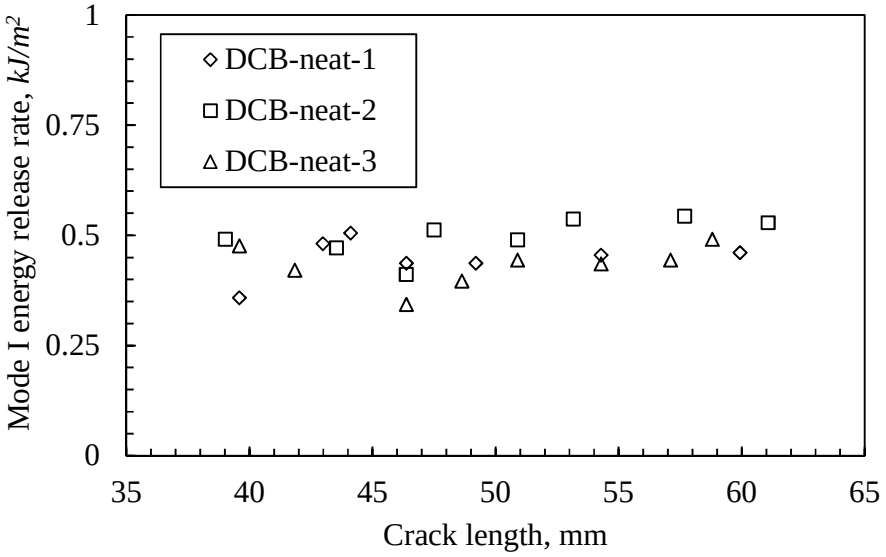

a.

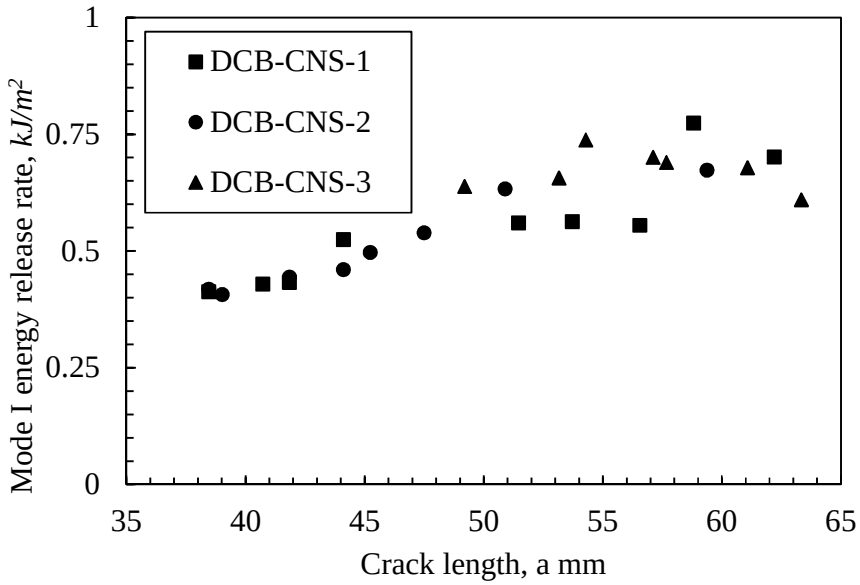

b.

Figure 5. Mode I energy release rate as a function of crack length: (a) neat DCB specimens; (b) DCB specimens modified with CNS-BP

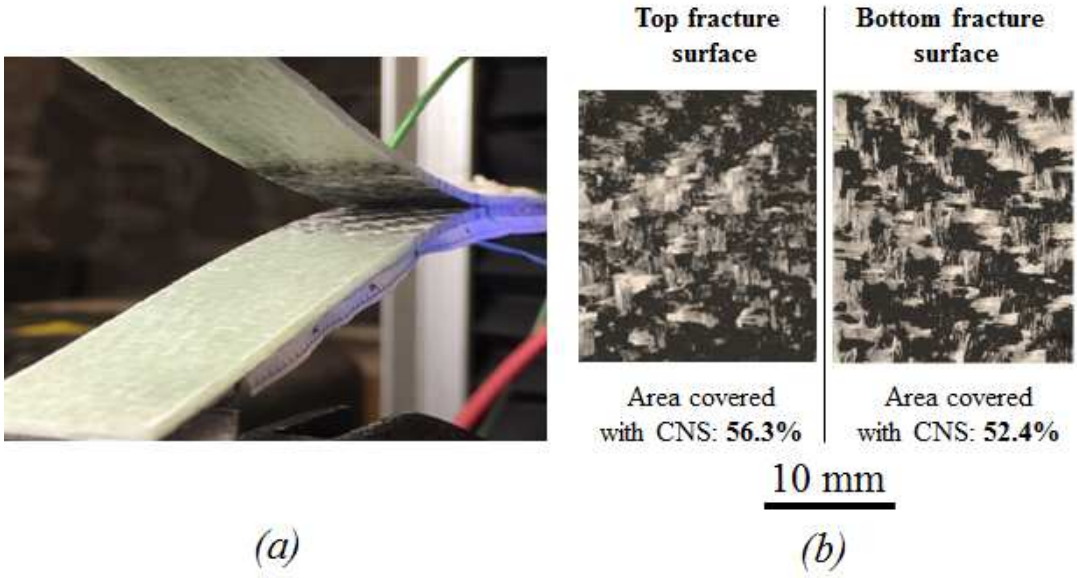

Figure 6. Cohesive fracture in DCB sample (a); image processing for calculating cohesive area on top and bottom fracture surfaces (b)

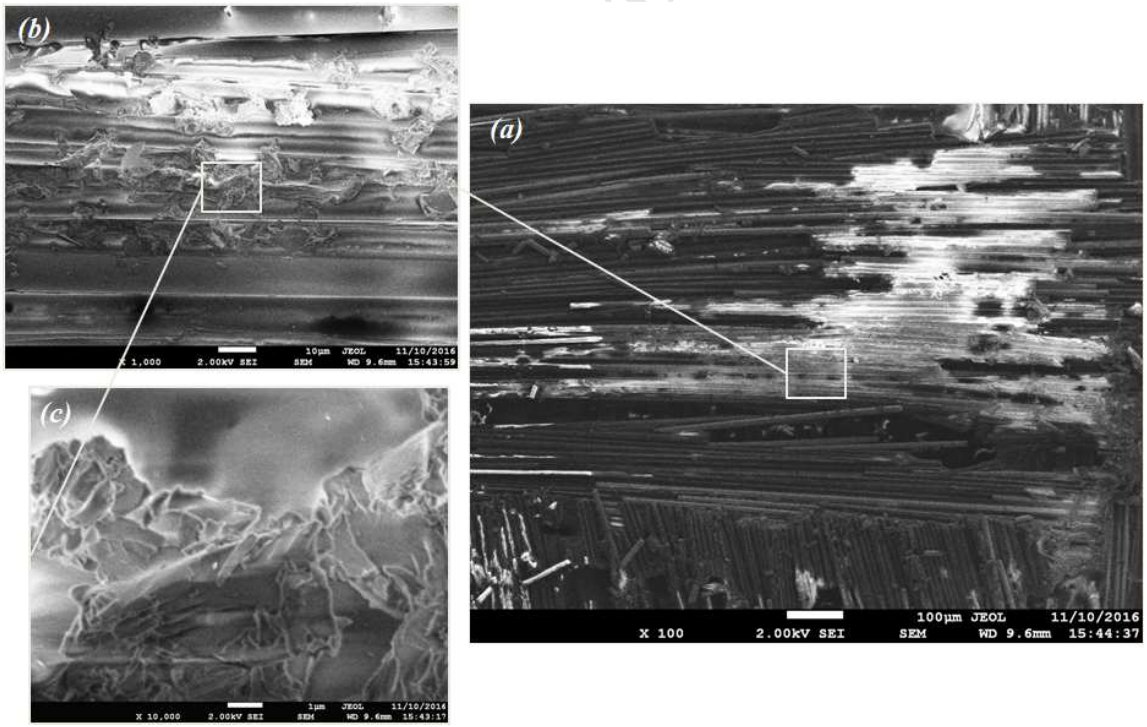

Figure 7. Microscopic view of the fracture surface: cohesive/adhesive fracture surface (a) with CNS agglomerates (b, c)

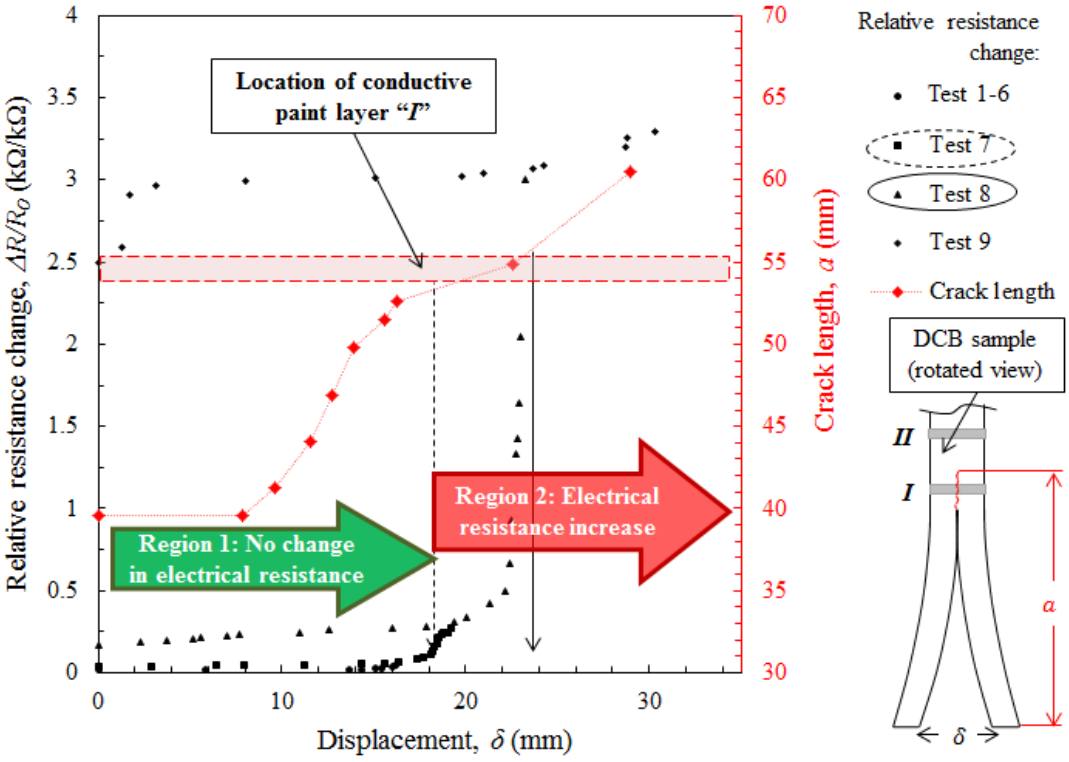

Figure 8. Relative resistance change recorded during crack propagation in mode I testing

Highlights:

- A new approach of incorporating carbon nanostructures, CNS, in the interlaminar region of glass fiber reinforced composite was proposed using frictional roller sliding of the buckypaper films
- Interlaminar toughness properties on composite were improved by cohesive failure of the CNS layer
- Changes in the electrical resistance of composite were observed with crack propagation enabling damage monitoring functionality